Development of Ultra-Fine Grained Structure in an Al-5.4%Mg-0.5%Mn Alloy Subjected to Severe Plastic Deformation*

Ilya Nikulin, Alla Kipelova, Sergey Malopheyev and Rustam Kaibyshev

Belgorod State University, Pobeda 85, Belgorod 308015, Russia

It was shown that extensive grain refinement takes place in an as-cast Al-5.4%Mg-0.5%Mn-0.1%Zr alloy subjected to severe plastic deformation under multi-directional forging up to a total true strain of ~9 at 250 and 300°C. At a strain of ~3, the deformed microstructure is mainly characterized by the formation of new grains along original boundaries and the development of well-defined subgrains within interiors of original grains. Upon further straining the misorientation of deformation-induced boundaries increases; new grains appear homogeneously both within grain interiors and along original boundaries. Decreasing temperature accelerates the transformation of low-angle boundaries (LABs) into high-angle boundaries (HABs). The resulted grain size evolved in this alloy was slightly less than that produced in an Al-6%Mg-0.35%Sc by severe plastic deformation under similar conditions. In addition, in the alloy belonging to Al-Mg-Mn-Zr system the formation of a fully recrystallized structure was found at a lower cumulative strain in comparison with the alloy belonging to Al-Mg-Sc system. This unusual difference associated with the fact that the Al-5.4%Mg-0.5%Mn-0.1%Zr alloy was initially subjected to solution treatment at a relatively low temperature of ~360°C. Effect of homogenization annealing on phase composition of this alloy is discussed.
[doi:10.2320/matertrans.L-MZ201115]

1. Introduction

There is currently a significant commercial interest in the development of non-heat treatable aluminum alloys with a submicrocrystalline (SMC) structure for structural applications.[1)] It is well-known that extensive grain refinement to the submicron range of grain size leads to significant increase in strength of none-age hardenable aluminum alloys at room temperature; ductility retains at sufficiently high level. At high and intermediate temperatures, ultra fine grained Al-Mg alloys may exhibit extraordinary high superplastic ductilities at high strain rates, typically in the range of $\sim 10^{-2}$–1 s^{-1}.[1)] It is now well established that a substantial reduction in the grain size of aluminum alloys can be easily attained through severe plastic deformation (SPD).[2)] Several SPD techniques, such as equal channel angular pressing (ECAP),[3,4)] accumulative roll bonding (ARB),[5,6)] and multi-directional forging (MDF),[9)] are mostly used for processing of aluminum alloys to produce SMC structures. These methods can impose a large amount of plastic deformation required for the occurrence of grain refinement in aluminum alloys.

The general features of the microstructure evolved during SPD in different aluminum alloys were examined in numerous works. It was reported,[2)] that the formation of a SMC structure can occur by the extension and compression of the initial grain boundaries followed by the discontinuous formation of transverse high-angle boundaries HABs. Other investigations have emphasized the role of continuous dynamic recrystallization (CDRX) in grain refinement under SPD of aluminum alloys at elevated and high temperatures.[3,8,9)] This process associates with the formation of low angle boundaries at low strains and their gradual transformation into high angle ones with further straining due to accumulation of lattice dislocations within deformation-induced boundaries.[3,7–10)] New grains result from the gradual increase in misorientation between subgrains during plastic deformation.[3,8,9)] It is worth noting that CDRX was found to be the mechanism of extensive grain refinement during ECAP,[8,9)] and MDF,[7)] in an Al-Mg-Sc alloy containing nanoscale coherent Al_3Sc particles. It was assumed that the coherent dispersoids provide the excellent stability of deformation-induced arrays of LABs that is a prerequisite condition for the completion of CDRX process.[7–10)] As a result, these alloys can be processed in semi-finished products with a very high strength and sufficient ductility. This unique combination of strength and ductility, which typically have opposing characteristics, is attributed mainly to the formation of the ultra-fine grained structure under SPD.[1)] In the same time, typical commercial alloys belonging to 5XXX series contain no Sc additives which are essentially expensive. Additives of Cr or Zr provide the formation of nanoscale dispersoids of Al_7Cr or Al_3Zr, respectively, in these alloys. In addition, these alloys contain manganese forming relatively coarse particles of Al_6Mn with plate-like shape. It is extremely important to develop a commercial viable route of thermomechanical processing (TMP) that may provide the formation of a fully recrystallized structure in semi-finished products from these alloys. This is not a trivial task due to the fact that aforementioned dispersoids are not effective in stabilizing arrays of deformation-induced boundaries that is a critical condition for extensive grain refinement.[9)] Therefore, a new approach to heat treatment of these alloys, which provides the formation of nanoscale dispersion being stable under TMP conditions, has to be developed.

The present study was initiated to demonstrate the potential of homogenization annealing at intermediate temperatures followed by MDF in producing a SMC structure in a commercial Al-5.4%Mg-0.5%Mn-0.1%Zr alloy designated as 1561 in Russia and denoted as 1561 Al, herein.

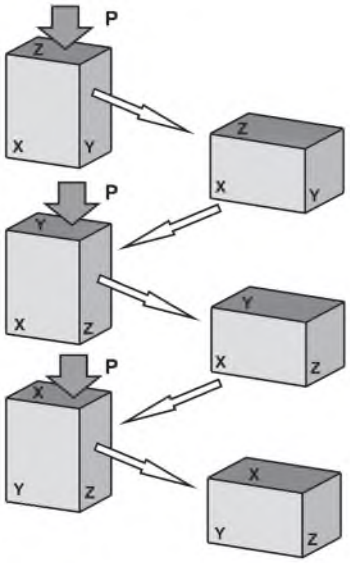

Fig. 1 Schematic illustration of one step of MDF consisted of three sequential compressions.

Specific attention was paid to the effect of pressing temperature and total imposed strain on deformation structure in an attempt to develop an optimal TMP route for extensive grain refinement in bulk billets of the 1561 Al that is highly important for commercial use in shipbuilding industry.

2. Material and Experimental Procedure

The commercial 1561 Al with a chemical composition of Al-5.43%Mg-0.52%Mn-0.1%Zr-0.12%Si-0.014%Fe (in mass%) was manufactured by direct chill casting and, then, annealed at 360°C for 6 h. Samples for MDF having rectangular shape with dimensions of $16 \times 14 \times 10\,\text{mm}^3$ were machined from homogenized ingots. The multi-directional forging of the 1561 Al was carried out at temperatures of ~250 and ~300°C at an initial strain rate of $\sim 10^{-2}\,\text{s}^{-1}$ using an Instron 300LX testing machine. A powder of boron nitride was used as a lubricant. The billets were compressed to a true strain (ε) of ~0.5 at each pass of MDF. The loading direction (P) was changed to 90° from pass to pass along three orthogonal directions (Fig. 1). Each step of MDF consisted of three sequent changes of compression axis from x direction to y direction and to z direction (Fig. 1) with a cumulative strain of ~1.5. New step of the MDF was started by compression along x axis again. The samples were deformed to several cumulative strains ($\Sigma\varepsilon$) of ~0.5, 1.5, 3, 6 and 9. Between passes the samples were reheated and held at a deformation temperature for ~10 min in order to reach a thermal equilibrium. This short dwelt time was necessary to prevent static recovery. Finally, the samples were water quenched. In order to determinate the influence of static annealing on deformed microstructure the samples strained to $\Sigma\varepsilon \approx 1.5$ and 6 were annealed for ~10 minutes at 250 and 300°C.

Following MDF, the specimens were cut from the central area of the forged billets parallel to X-plate for microstructural observations. For the electron-backscattering diffraction (EBSD) analysis these specimens were slightly electropolished to give a strain-free surface. EBSD orientation maps were recorded using a FEI Quanta 600FEG scanning electron microscope equipped with a high-resolution EBSD analyzer. The arbitrary area was automatically scanned with a step size of 0.1 µm. In the data presented, HABs were defined as $\theta \geq 15°$ in misorientation and LABs as $2° < \theta < 15°$. HABs and LABs are depicted in EBSD maps as black and white lines, respectively. Thin foils were examined using a JEM-2100 transmission electron microscope (TEM) operating at 200 kV that was equipped with an INCA energy-dispersive X-ray spectrometer. Particles were identified using data of semi-automatic energy dispersive X-ray spectroscopy (EDX)-analysis and analysis of diffraction patterns. The dislocation density was measured in accordance with procedure described in previous work.[3)]

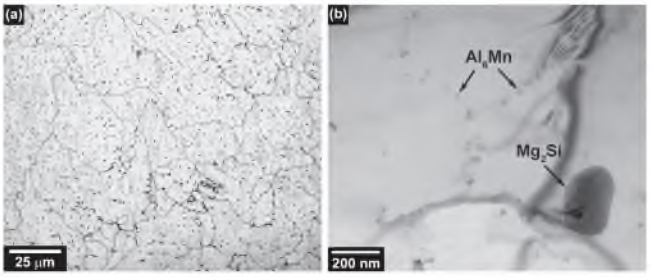

Fig. 2 Initial microstructure of the 1561 Al after annealing at 360°C for 6 h: (a) optical microscopy, (b) TEM image.

3. Experimental Results

3.1 Macrostructure after homogenization annealing

Microstructure of the homogenized 1561 Al consists of roughly equiaxed grains with an average size of ~250 µm (Fig. 2(a)). Two types of second phase particles were revealed by EDX analysis in resulted structure. First one is relatively coarse Mg_2Si and Al_3Mg_2 particles with an average size of ~200 nm (Fig. 2(b)). Second one is fine dispersoids of Al_6Mn with an average size of ~25 nm (Fig. 2(b)). In addition, the present alloy was carefully examined in TEM with respect to the formation of Al_3Zr dispersoids during annealing at 360°C. However, no Al_3Zr dispersoids were revealed. It was shown that annealing at 450°C at least for 200 h is necessary for precipitation of fine Al_3Zr dispersoids in this type of aluminum alloy.[11)] Thus, a dispersion of nanoscale Al_6Mn particles having equiaxed shape evolved under homogenization annealing; Zr retained within supersaturated solid solution after homogenization annealing at the intermediate temperature.

3.2 Microstructure evolved at 250°C

Typical EBSD maps of the deformation structures are shown in Fig. 3. Microstructure developed after $\Sigma\varepsilon \approx 0.5$ is mainly characterized by extensive elongation of initial grains; extended deformation-induced boundaries are evolved within interiors of these grains. The new boundaries having low-to-moderate and even high angle misorientations are mainly formed along shear direction. Figure 4 represents the distribution of typical point-to-point ($\Delta\theta$) and cumulative point-to-origin ($\Sigma\Delta\theta$) misorientations developed in the 1561

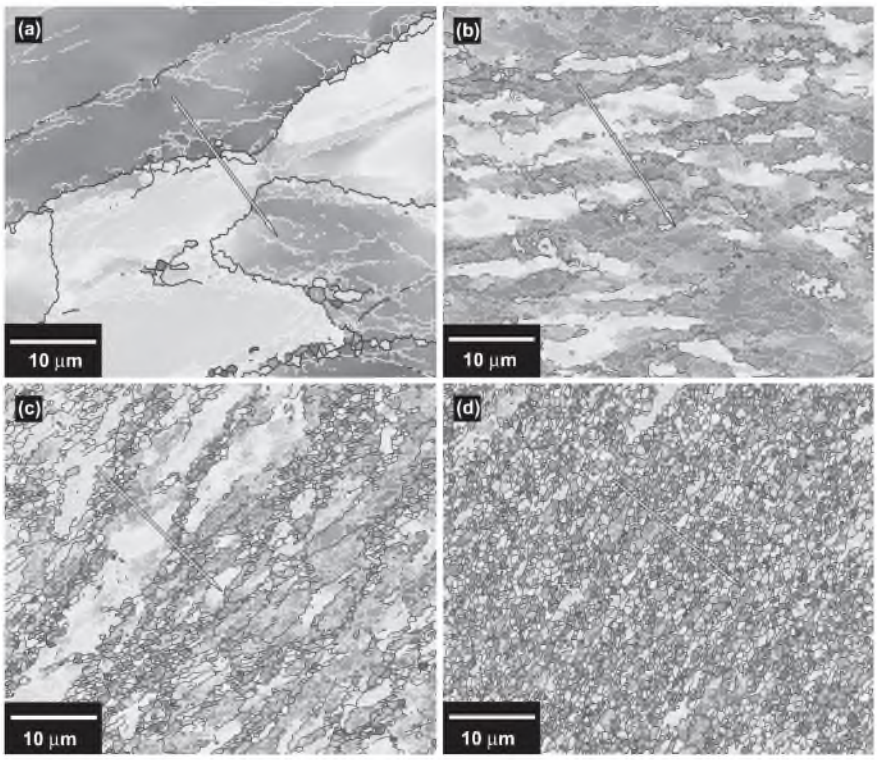

Fig. 3 Typical EBSD maps of the 1561 Al processed by MDF at 250°C to various strains: (a) $\Sigma\varepsilon \approx 0.5$, (b) $\Sigma\varepsilon \approx 1.5$, (c) $\Sigma\varepsilon \approx 3$, (d) $\Sigma\varepsilon \approx 9$.

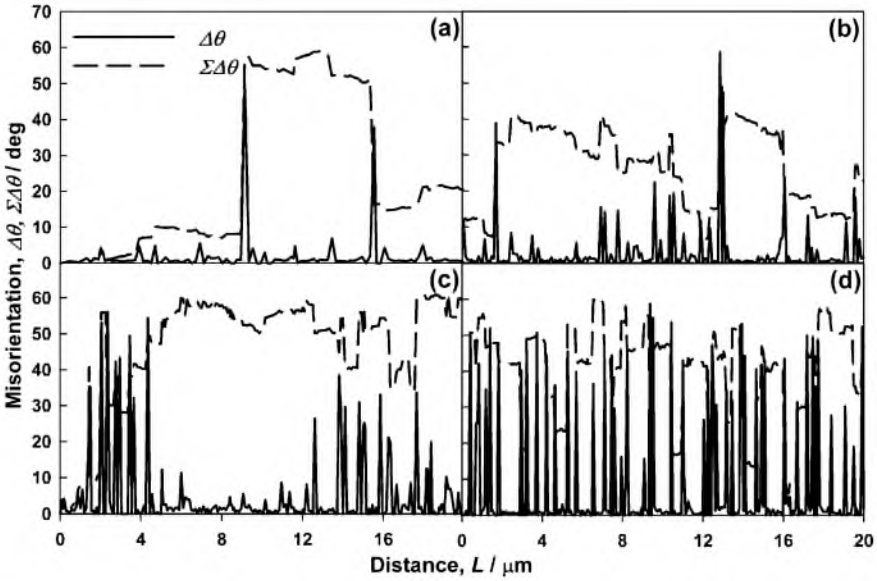

Fig. 4 Point-to-point ($\Delta\theta$) and point-to-origin ($\Sigma\Delta\theta$) misorientation of strain-induced boundaries developed along lines pointed at Fig. 3: (a) $\Sigma\varepsilon \approx 0.5$, (b) $\Sigma\varepsilon \approx 1.5$, (c) $\Sigma\varepsilon \approx 3$, (d) $\Sigma\varepsilon \approx 9$.

Al along the lines indicated in Fig. 3. The values of $\Delta\theta$ and $\Sigma\Delta\theta$ define the misorientations evolved by 0.1 μm steps relative to the previous point and to the first point, respectively. It can be seen (Fig. 4(a)) that $\Delta\theta$ does not exceed 2° except for some values with $\Delta\theta > 3°$, which correspond to the deformation-induced dislocation boundaries. There is evidence for continuous misorientations appeared between extended deformation-induced low-to-moderate angle boundaries. These lattice distortions can be attributed to the dislocation tensor and is indicative for deformation gradient at such areas at low strain. It is worth noting that newly evolved grains appeared in the vicinity of triple junction and along the original grain boundaries. Increasing of cumulative strain to $\Sigma\varepsilon \approx 1.5$ leads to increasing number of deformation-induced boundaries (Fig. 3(b)) as well as their misorientation. Average distance between deformation-induced boundaries decreases significantly, and the continuous misorientation between them

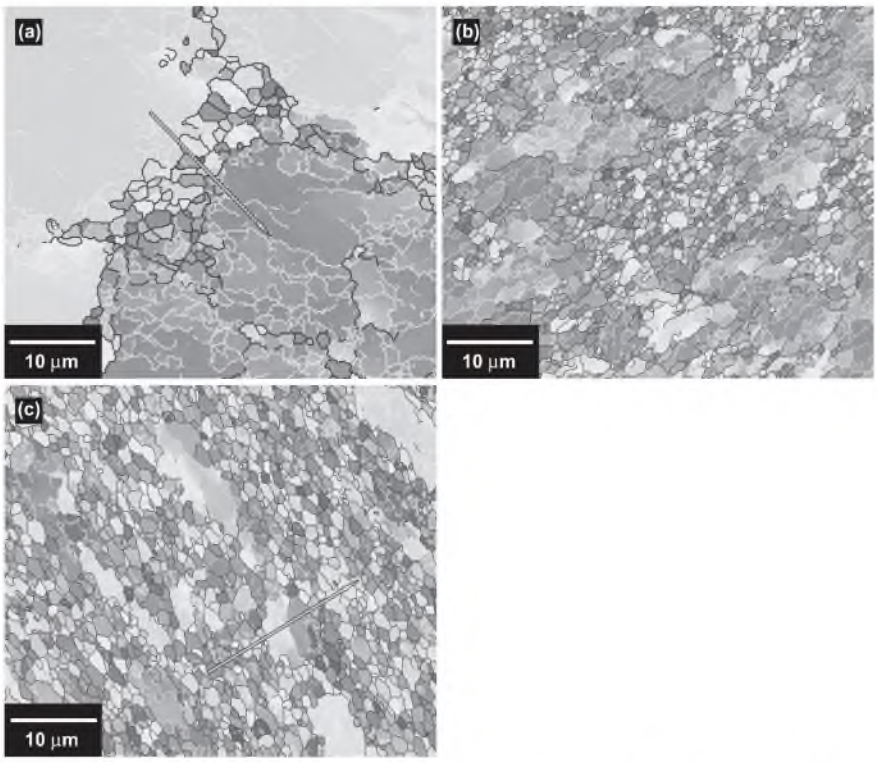

Fig. 5 Typical EBSD maps of the 1561 Al processed by MDF at 300°C to various strains: (a) $\Sigma\varepsilon \approx 1.5$, (b) $\Sigma\varepsilon \approx 3$, (c) $\Sigma\varepsilon \approx 9$.

increases (Fig. 4(b)). Microstructure evolved at $\Sigma\varepsilon \approx 1.5$, is mainly characterized by a homogeneous distribution of dislocation cells or recovered subgrains with boundaries having low-to-moderate misorientations as seen in Fig. 4(b). Upon further straining to $\Sigma\varepsilon \approx 3$ the misorientations of deformation-induced boundaries increase; new grains outlined by HABs are evolved inhomogeneously (Fig. 3(c)). Colonies of these grains adjoined with areas of original grains containing highly deformed cell structure subdivided by LABs with $\theta < 5^\circ$ (Fig. 4(c)). In the same time the continuous misorientations between these boundaries decrease (Fig. 4(c)). Deformation up to $\Sigma\varepsilon \approx 6$ provides an increase in number of new grains; the formation of recovered subgrains occurs within interiors of original grains. Deformation to higher strains increases number of true ultrafine grains. As a result, at $\Sigma\varepsilon \approx 9$, the microstructure developed mainly consists of the fine recrystallized grains separated by HABs (Fig. 3(d)); the continuous misorientations within these grains are insignificant (Fig. 4(d)). However, a low number of subgrains could be found even at $\Sigma\varepsilon \approx 9$.

3.3 Microstructure evolved at 300°C

Typical EBSD maps of the deformation structures are shown in Fig. 5. At $\Sigma\varepsilon \approx 1.5$, arrays of LABs evolve within interiors of initial grains, and new grains are formed near original grain boundaries (Fig. 5(a)). At 300°C, the main feature of deformation structure is the formation of separate areas of recrystallized grains at all cumulative strains (Fig. 5). It can be seen (Fig. 6(a)) that $\Delta\theta$ and $\Sigma\Delta\theta$ profiles are almost the same as in the microstructure developed at 250°C and $\Sigma\varepsilon \approx 0.5$ (Fig. 4(a)). The difference between these profiles consists in the lacking of the continuous

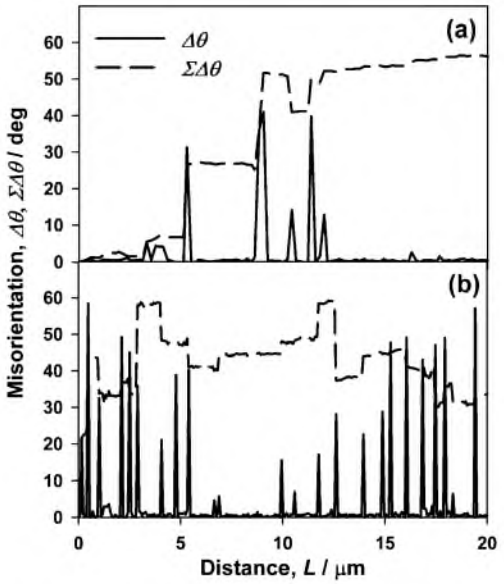

Fig. 6 Point-to-point ($\Delta\theta$) and point-to-origin ($\Sigma\Delta\theta$) misorientation of strain-induced boundaries developed along lines pointed at Fig. 5: (a) $\Sigma\varepsilon \approx 1.5$, (b) $\Sigma\varepsilon \approx 9$.

misorientation within crystallites evolved at a temperature of 300°C. At $\Sigma\varepsilon \approx 3$, areas of recrystallized grains alternate with areas of subgrains (Fig. 5(b)); sizes of grains and subgrains are nearly the same. The fraction of new grains increases with increasing strain. At $\Sigma\varepsilon \approx 9$, bands of true grains outlined by HABs alternate with unrecrystallized areas which subdivided on coarse subgrains (Fig. 5(c)). The continuous misorientation within these grains and subgrains

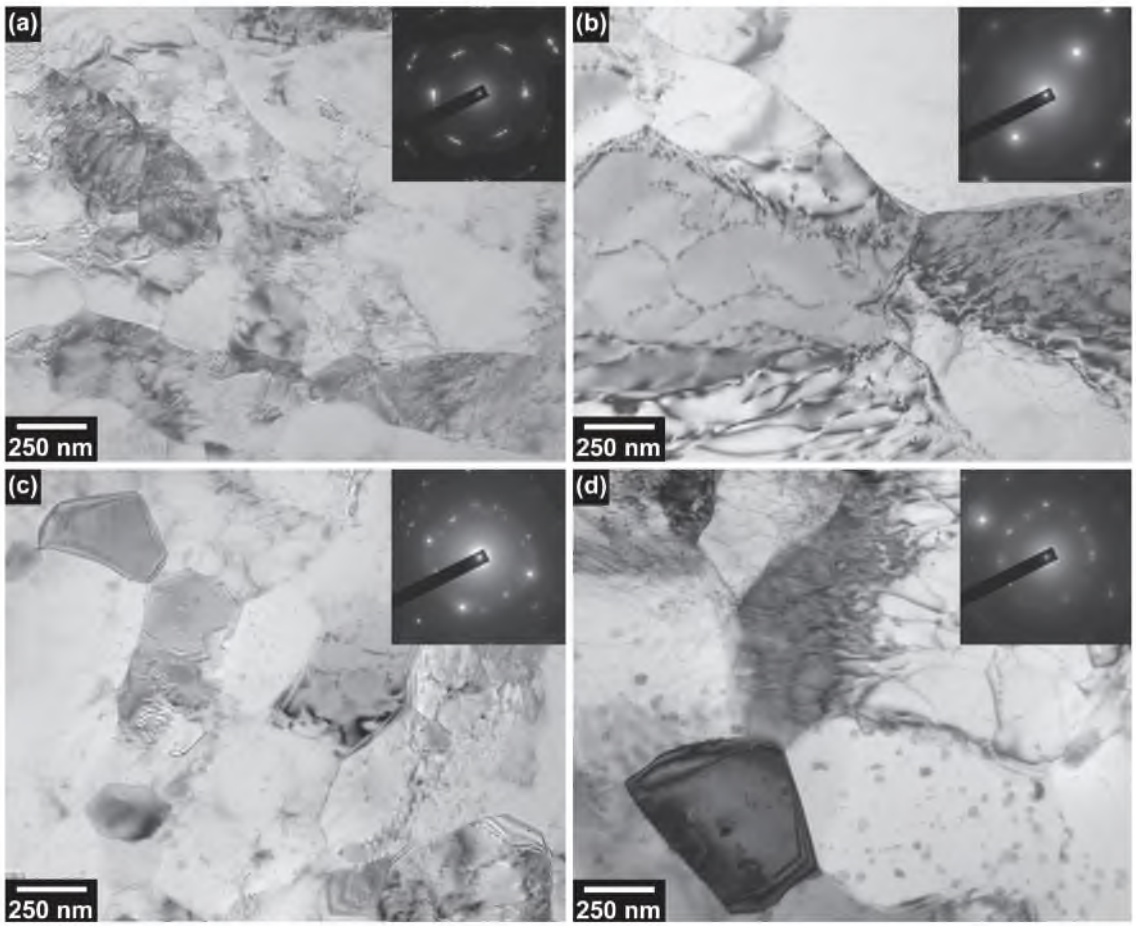

Fig. 7 Typical TEM structure and associated SAED patters for 1561Al deformed at 250 (a), (c) and 300°C (b), (d) to $\Sigma\varepsilon \approx 1.5$ (a), (b) and $\Sigma\varepsilon \approx 9$ (c), (d).

Table 1 Dislocation density measured in the 1561 Al processed by MDF and MDF followed by annealing.

	$T = 250$°C	$T = 300$°C
$\Sigma\varepsilon \approx 1.5$	1.6×10^{14}	2.9×10^{13}
$\Sigma\varepsilon \approx 1.5$ + annealing for ~10 min	0.9×10^{14}	1.7×10^{13}
$\Sigma\varepsilon \approx 6$	6.2×10^{13}	4.9×10^{13}
$\Sigma\varepsilon \approx 6$ + annealing for ~10 min	4.5×10^{13}	3.5×10^{13}

are essentially the same (Fig. 6(b)). It is worth noting that size of the subgrains is higher than that of the grains (Figs. 5(c) and 6(b)) by a factor of ~5.

3.4 TEM microstructure

Typical microstructure revealed by TEM in the 1561 Al strained at low and high strains are represented in Fig. 7. At 250°C and low strains, the deformation microstructure consists of coarse elongated subgrains (Fig. 7(a)) containing high density of lattice dislocations (Table 1). The misorientation of these subgrain boundaries was evaluated as ~10–15° by analysis of selected area electron diffraction (SAED) pattern. Further straining provides gradual increase in misorientation of deformation-induced boundaries; subgrains containing high dislocation density transform into recovered subgrains and new grains containing moderate density of lattice dislocations; dislocation free grains can be observed (Fig. 7(c)).

Deformation microstructure developed at 300°C is rather different from those evolved at 250°C, as can be seen in Fig. 7. At $\Sigma\varepsilon \approx 1.5$, coarse subgrains with a size of ~1.3 μm containing moderate number of lattice dislocations are developed (Table 1); misorientation of their boundaries is typically less than 5° (Fig. 7(b)). However, at 300°C and $\Sigma\varepsilon \approx 1.5$, recovered subgrains with low number of dislocations can be also found. Increasing strain results in development of grained structure (Fig. 7(d)) nevertheless the high number of lattice dislocations appears even at $\Sigma\varepsilon \approx 9$.

It is also to note that at both temperatures, numerous Al_6Mn dispersoids precipitated in deformed structure at moderate to high strains (Fig. 7) additionally to those observed after homogenization annealing at 360°C. These particles effectively pin mobile dislocations as during high temperature creep.[12] It seems that the nanoscale Al_6Mn dispersoids precipitate heterogeneously on lattice dislocations (Fig. 7(b)). Deformation temperature strongly affects the size of these dispersoids. At 300°C, particles with an average size of ~23 nm precipitate during deformation (Figs. 7(b) and 7(d)). In contrast, at 250°C, the precipitation of the particles with an average size of ~10 nm is observed

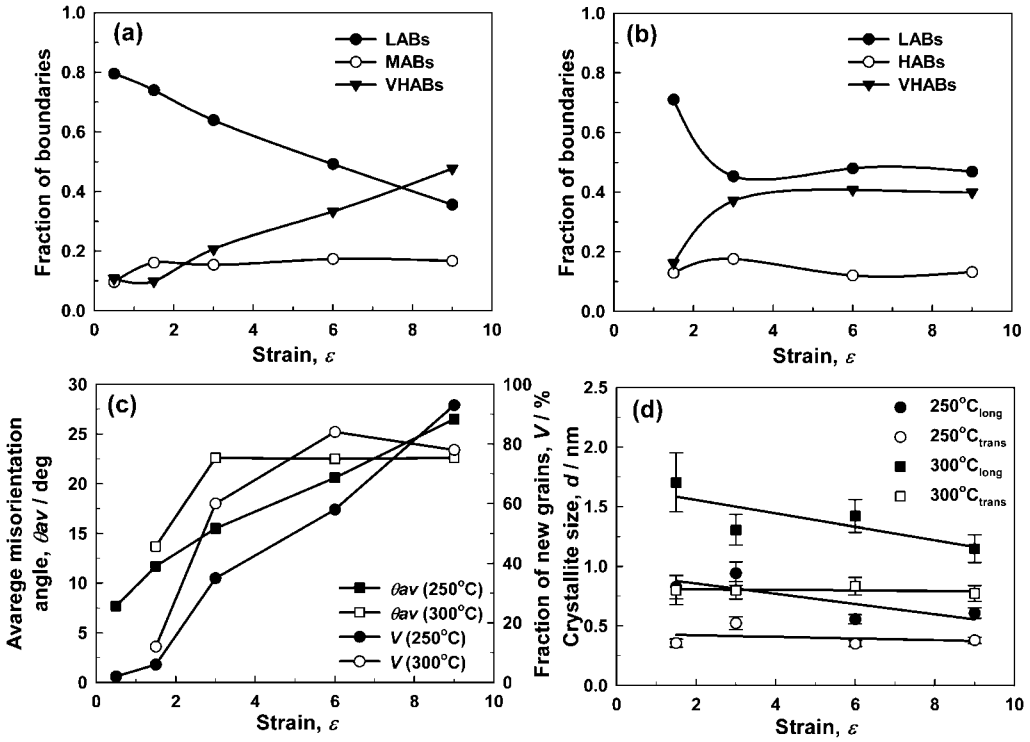

Fig. 8 Effect of strain on (a), (b) population of LABs, MABs and VHABs; (c) average misorientation of deformation-induced boundaries, θav and fraction of recrystallized grains, V; (d) the crystallite size, d.

(Figs. 7(a) and 7(c)). Thus, at 250°C, upon straining the precipitation of Al_6Mn dispersoids with size being significantly less than that precipitated under homogenization annealing takes place. It results in a significant increase in Zener drag pressure.[13)]

It is generally known that the Al alloys are normally considered to be "recovery materials", in which static recovery operating extensively at high temperature conditions can effectively decrease the dislocation density stored during deformation and suppress recrystallization.[13)] An important feature of the MDF is that the deformed samples inevitably undergo static annealing between MDF passes at elevated temperatures. Static recovery may decrease the strain gradients and/or strain heterogeneities throughout rearrangement of dislocations[13)] accumulated in each MDF pass at elevated temperatures and thus, retard grain refinement even at large strains imposed by MDF. However, in the present case short annealing performed before each MDF pass lead to minor changes in deformed structure both at low and at high strains. Size of the new crystallites developed at MDF remains almost unchanged during annealing ever at a temperature of ~300°C. For example, average crystallite size measured in samples deformed to $\Sigma\varepsilon \approx 6$ at 300°C and in this sample additionally annealed at the same temperature for ~10 min were of ~1.1 μm and ~1.3 μm, respectively. Therefore, recrystallization processes under interpass annealing give a minor contribution to microstructural evolution. The overall dislocation density was also almost the similar in strained and annealed conditions (Table 1) suggesting high stability of deformed structure against static recovery. Thus, a weak influence of static recovery on the grain refinement of the 1561 Al was found.

3.5 Parameters of microstructure as a function of strain

The effect of strain on the boundary fraction of the 1561 Al deformed at 250 and 300°C is shown in Figs. 8(a) and 8(b), respectively. It is worth noting that in this figure the HABs which were subdivided on medium angle (MABs) ($15 \leq \theta < 30°$) and very high angle grain boundaries (VHABs) ($30 \leq \theta < 62.8°$). At 250°C, in the strain interval 0.5–9 the fraction of LABs continuously decreases from 0.8 to 0.36 with increasing strain. While, at 300°C, in the stain interval 1.5–3 the fraction of LABs decreases from 0.71 to 0.45 and remains virtually unchanged with further straining (Fig. 8(b)). Strain increase to $\Sigma\varepsilon \approx 9$ insignificantly affects the fraction of MAGBs which is almost unchanged during deformation both at 250 and 300°C as well. At 250°C, the fraction of VHABs continuously increases with increasing cumulative strain; at $\Sigma\varepsilon \approx 9$, the sum of MAGBs and VHABs is ~0.64. On the other hand, at 300°C, the fraction of VHABs increases up to $\Sigma\varepsilon \approx 3$ and remains unchanged (~0.4) in the strain interval 3–9.

Strain dependence of the average misorientation (θav) and volume fraction of new recrystallized grains, are summarized in Fig. 8(c). It can be seen that at 250°C, the average misorientation increases rapidly from 7.7 to 15.4° in strain interval from 0.5 to 3 and then gradually increases to 26.5° upon further straining to $\Sigma\varepsilon \approx 9$. At 250°C, the volume fraction of new grains increases slowly up to $\Sigma\varepsilon \approx 1.5$; extensive increase in this volume fraction starts to occur at higher strain. A rapid increase in the average misorientation and the fraction of recrystallized grains is associated with the formation of new HABs. However, at 250°C, the average misorientation and the volume fraction of new grains do not approach a saturation value even at $\Sigma\varepsilon \approx 9$. At 300°C,

average misorientation increases rapidly at $\Sigma\varepsilon \leq 3$, and approaches saturation value of ~22.5° in the strain interval 3–9. Fraction of new grains increases greatly at $\Sigma\varepsilon \leq 3$; upon further strain an increase in this fraction occurs slowly. Slight decrease in the fraction of new grains at $\Sigma\varepsilon \approx 9$ was associated with restoration processes occurring during intermediate annealing between MDF passes. It is worth noting that continuous increase in the average misorientation in the present alloy takes place due to increasing VHABs portion with strain.

Effect of strain on the average crystallite size measured in longitudinal direction (*i.e.* in the direction of elongated grains) and in the transverse direction are summarized in Fig. 8(b). It is seen that longitudinal size of crystallites tends to decrease gradually with increasing strain at both temperatures, while transversal size does not change significantly. The size of new grains increases with increasing temperature. At 250 and 300°C and, the average size of new grains was ~0.5 μm and ~1 μm, respectively after cumulative strain of $\Sigma\varepsilon \approx 9$. Effect of temperature on size of subgrains evolved within unrecrystallized areas is the same.

4. Discussion

4.1 Role of homogenization annealing

Inspection of experimental data shows that microstructure evolution in the 1561 Al under severe plastic deformation by MDF is similar to that in Sc-bearing aluminum alloys.[3,7–9,14] It is caused by the fact that homogenization annealing at intermediate temperature provides the formation of a dispersion of nanoscale particles of Al_6Mn. In the 1561 alloy the incoherent nanoscale particle of Al_6Mn precipitated during annealing at a relatively low temperature of 360°C. No high temperature solution treatment at a temperature of 500°C was performed. Therefore, it seems that the use of relatively low temperature of homogenization annealing is extremely important for the formation of ultrafine grained under subsequent SPD.

It is obvious that the presences of these dispersoids are a prerequisite condition for occurrence of CDRX in Al-Mg alloys. No evidence for precipitation of Al_3Zr phase was found both under homogenization annealing and severe plastic deformation as well. Therefore, Zr retains within solid solution hinders diffusion, significantly. This fact results in two sequences affecting positively CDRX occurrence. First, ability of dislocation to climb controlled by lattice diffusion is decreased. Second, dispersoids of Al_6Mn phase showed high resistance to coarsening. The Al_6Mn particles retain their nanoscale size and do not acquire plate-like shape both under homogenization annealing and severe plastic deformation as well. As a result, these dispersoids exert high Zener drag force,[13] providing final size of recrystallized grains less than in an Al-Mg-Sc alloy.[7–9] It is known that the formation of the SMC structure in Al-Mg alloys is highly facilitated by the presence of nanoscale particles of $Al_3(Sc,Zr)$. It is turned out that dispersion of nanoscale incoherent Al_6Mn particles having equiaxed shape is more effective in stabilizing arrays of deformation-induced boundaries in comparison with coherent nanoscale dispersoids of Al_3Sc phase.[7–9] We can presume that the formation of three-dimensional arrays of LABs in the 1561 Al leads to refinement of Al_6Mn dispersoids in comparison with coarsening of $Al_3(Sc,Zr)$ particles in an Al-6%Mg-0.35%Sc alloy designated as 1570 Al.[9] In addition, precipitation of particles of Al_6Mn on dislocations during SPD also gives a significant contribution in achieving finest grain size in this Al-Mg alloy. This is why at 300°C, the resulted grain size in the 1561 Al is less than that in the 1570 Al.[7–10]

4.2 Strain-induced grain formation process

Extensive grain refinement in the 1561 Al occurs through CDRX, which was elsewhere found to be operative in the 1570 Al.[7–10] Regularities of CDRX process in the 1561 Al and 1570 Al are almost the same. CDRX consists of two sequential processes: the formation of three-dimensional arrays of LABs and the gradual transformation of LABs into HABs. At initial stages of deformation ($\varepsilon \leq 1.5$) the three-dimensional arrays of LABs are developed in original grain interiors due to the formation of deformation-induced boundaries. Initially, separate LABs form roughly parallel to shear direction. Next, the formation of LABs in transverse direction results in appearance of arrays of LABs. Upper further strain the subgrains elongate, and their boundaries acquire misorientations of $5 \leq \theta \leq 15°$. It is obvious that at $\Sigma\varepsilon \geq 3$, the recrystallized grains persistently replace subgrains through continuous transformation of LABs to HABs. Upon processing to a cumulative strain of $\Sigma\varepsilon \approx 9$, the average misorientation rapidly increases to 26.5° and 22.6° for 250 and 300°C, respectively (Fig. 8(c)). It is seems that at 250°C, dislocation rearrangement within the interiors of initial grains is hindered; high density of LABs is attained after a strain of ~3 (Fig. 9(a)). High number of mobile dislocations move across subgrain interiors and are trapped by deformation-induced LABs resulting in an increase in their misorientation followed by their conversation to HABs at 250°C. At high strain, the fraction of HABs of ~0.64 exceeds a threshold value of ~0.6 for conventional grained structures.[2] It is obvious that this structure is a granular one, and it is possible to conclude that the almost fully recrystallized structure developed at 250°C under MDF to a moderate cumulative strain of ~9 in the 1561 Al.

At 300°C, the transformation of LABs into HABs occurs with lower rate attaining saturation at $\Sigma\varepsilon \approx 3$. It seems that this fact is associated with significant dislocation annihilation due to increased ability of lattice dislocations to re-arrangements by climb rather than low stability of arrays of deformation induced LABs. Under straining the nanoscale dispersoids of Al_6Mn is highly effective in stabilization both

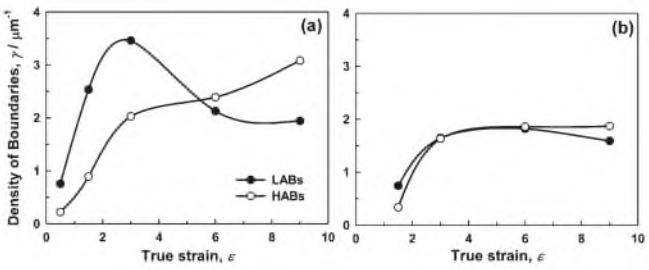

Fig. 9 Effect of strain on density of deformation-induced boundaries (a) 250°C and (b) 300°C.

LABs and HABs as it was discussed above. Therefore, at this temperature, the formation of three-dimensional arrays LABs is a key factor controlling CDRX kinetic. Low density of LABs evolved (Fig. 9(b)) reduces the rate of CDRX. As a result, the formation of a fully recrystallized structure do not observed even at a cumulative strain of $\Sigma\varepsilon \approx 9$.

In addition, it is worth noting that the formation of a fully recrystallized structure in the 1561 Al was found at lower cumulative strain in comparison with the 1570 Al.[8,9] Perhaps, it is caused by the fact that high volume fraction of coherent $Al_3(Sc,Zr)$ hinders the formation of well-defined subgrain structure at lower strains in the 1570 Al. Fast evolution of ultrafine grained structure under SPD in the 1561 Al is attributed to the optimal combination of size, volume fraction and incoherent nature of interface boundaries of nanoscale dispersoids that exerts an optimal values both of Zener drag force and pinning pressure for dislocation glide. Thus, the combination of homogenization annealing at intermediate temperature with MDF provides the formation of submicrometer scale grains in the 1561 Al which contains no Sc additions at moderate strains.

5. Summary

The present study demonstrates the feasibility of achieving extensive grain refinement in the commercial 1561 aluminum alloy through combination of homogenization annealing at an intermediate temperature of 360°C followed by multi-directional forging.

(1) Homogenization annealing at 360°C leads to precipitation of nanoscale dispersoids of Al_6Mn with average size of ~25 nm and equiaxed shape; Zr retains within the supersatured solid solution providing high coarsening resistance of the Al_6Mn at $T \leq 300$°C.

(2) Under severe plastic deformation the additional precipitations of nanoscale Al_6Mn particles takes place on dislocations. Their size is ~10 and ~23 nm at 250 and 300°C, respectively.

(3) At temperatures of ~250 and 300°C, extensive grain refinement takes place in the 1561 Al subjected to MDF. The average size of recrystallized grains is ~0.5 and ~1 μm at 250 and 300°C, respectively.

(4) Decreasing temperature accelerates the transformation of LABs into HABs. At 250°C, a fully recrystallized structure was observed in samples subjected to MDF with a total cumulative strain of $\Sigma\varepsilon \approx 9$. At 300°C, the formation of partially recrystallized structure is observed even after $\Sigma\varepsilon \approx 9$.

Acknowledgements

This study was supported by Federal Agency for Education, Russia, under grant No. P1735. Authors are grateful to staff of Joint Research Center, Belgorod State University, for their assistance with computational and instrumental analysis.

REFERENCES

1) R. Z. Valiev and T. G. Langdon: Prog. Mater. Sci. **51** (2006) 881–981.
2) F. J. Humphreys, P. B. Prangnell, J. R. Bowen, A. Gholinia and C. Harris: Phil. Trans. R. Soc. Lond. A **357** (1999) 1663–1680.
3) R. Kaibyshev, K. Shipilova, F. Musin and Y. Motohashi: Mater. Sci. Eng. A **396** (2005) 341–351.
4) Y. Iwahashi, Z. Horita, M. Nemoto and T. G. Langdon: Acta Mater. **46** (1998) 3317–3331.
5) Y. Saito, N. Tsuji, H. Utsunomiya, T. Sakai and R. G. Hong: Scr. Mater. **39** (1998) 1221–1227.
6) Y. Saito, N. Tsuji, H. Utsunomiya and T. Sakai: Acta Mater. **47** (1999) 579–583.
7) R. Kaibyshev, S. Olenyov and F. Musin: Mater. Sci. Forum **426–432** (2003) 4603–4608.
8) O. Sitdikov, T. Sakai, E. Avtokratova, R. Kaibyshev, Y. Kimura and K. Tsuzaki: Mater. Sci. Eng. A **444** (2007) 18–30.
9) O. Sitdikov, T. Sakai, E. Avtokratova, R. Kaibyshev, K. Tsuzaki and Y. Watanabe: Acta Mater. **56** (2008) 821–834.
10) T. G. Nieh, L. M. Hsiung, J. Wadsworth and R. Kaibyshev: Acta Mater. **46** (1998) 2789–2800.
11) Z. Jia, G. Hu, B. Forbord and J. K. Solberg: Mater. Sci. Eng. A **444** (2007) 284–290.
12) R. Kaibyshev, F. Musin, E. Avtokratova and Y. Motohashi: Mater. Sci. Eng. A **392** (2005) 373–379.
13) F. J. Humphreys and M. Hatherly: *Recrystallization and related annealing phenomena*, (Pergamon Press, Oxford, UK, 1996) pp. 304–306.
14) P. J. Apps, J. R. Bowen and P. B. Prangnell: Acta Mater. **51** (2003) 2811–2822.